Excitons in $Mg(OH)_2$ and $Ca(OH)_2$ from *ab initio* calculations

A. Pishtshev

Institute of Physics, University of Tartu, 51014 Tartu, Estonia

S. Zh. Karazhanov

Department for Solar Energy, Institute for Energy Technology, NO-2027 Kjeller, Norway

M. Klopov

Department of Physics, Tallinn University of Technology, 19086 Tallinn, Estonia

Abstract

By using *ab initio* calculations with the HSE06 hybrid functional and GW approximation combined with numerical solution of the Bethe Salpeter equation (GW-BSE) we predict the existence of diverse number of excitonic states in multifunctional hydroxides $X(OH)2$ ($X=$ Mg and Ca) that were not previously reported experimentally or theoretically. Imaginary part of the dielectric function and reflectivity spectra show very strong peaks corresponding to the electron-hole pair states of large binding energy. The origin of the excitons is attributed to strong localization of the hole and electron associated to oxygen $2p_x, 2p_y$ occupied states as well as to oxygen and earth metal s empty states, respectively. The results have important implications for different applications of the materials in optoelectronic devices.

Keywords: Magnesium hydroxide and calcium hydroxide, excitons, electronic structure, optical properties
PACS: 71.22.+i; 71.35.-y; 71.35.Cc

Email address: smagulk@ife.no (S. Zh. Karazhanov)

1. Introduction

Electronic many-body effects play a key role in the electrical and optical properties of solids [1, 2]. In particular, the proper accounting for two-particles excitation energies allows one to explain specific features of the optical absorption spectrum of semiconductors and insulators [3–5]. Due to specific features of dielectric screening, e.g., low dielectric constants, the interaction of the excited electrons and holes differs significantly in wide-gap insulators than that in semiconductors. Exciton binding energy resulting from the strong $e-h$ interaction is often of large magnitude [2]. In this context, the main focus of the present work is the principal case study demonstrating that the strength of the $e-h$ interaction can be modulated by materials engineering methods. For example, the experimentally established exciton binding energy is 86 meV for MgO and 95 meV for CaO with band gap of 7.775 eV and 7.034 eV [6], respectively: both materials possessing predominantly ionic type of chemical bonding. By means of hydration of these materials the existing ionic bonds are reorganized so that a certain portion of covalency is supplied by the water molecules H_2O. The resulting crystalline alkali-earth hydroxides $X(OH)2$ (X=Mg, Ca) acquire a system integrity that is governed by the negative oxygen ions via a bridging combination of the strong covalent bonding in the OH^- hydroxyl anions and $X-O$ strong ionic connections [7]. This in turn determines a multifunctionality property of $X(OH)2$ compounds, which is generally based on the equal utilization of electronic characteristics such as large band gap and low refractive index (relevant to purely ionic systems) and covalent contributions from the oxygen within a common crystal-chemical environment. Our preliminary considerations applied to $X(OH)2$ have shown that this feature contributes significantly to the nature of optoelectronic properties, so that one can expect in these materials strong Coulomb attraction between an excited electron and a hole and, consequently, generation of an exciton with a large binding energy. Excitonic contributions to the optical absorption process can be described by numerical solution of the Bethe-Salpeter equation (BSE) with high accuracy [1, 8–11]. In this work we will study the electronic structure and optical properties of $X(OH)2$ and report about band gap excitons with large binding energy of 0.46 eV for $Mg(OH)_2$ and 0.85 eV $Ca(OH)_2$. We identify and analyze the character of exciton peaks in the optical spectrum and relate them to strong localization of the hole and electron to oxygen $2p_x, 2p_y$ occupied states as well as to oxygen and metal s empty states, respectively. The fundamental aspect

of the article is that we have found that in crystalline hydroxides $Mg(OH)_2$ and $Ca(OH)_2$ the many-body effects in the optical absorption spectra play a crucial role. From a practical point of view, materials under consideration may serve as interesting hosts, so that our results definitely have important implication for different applications of the materials in optoelectronic devices [12–14].

2. Structural model and computational details

The multifunctional hydroxides $X(OH)2$ crystallize into the CdI_2-type structure of space group of D^3_{3d}(Refs. [15–17]) with the unit cell containing two metal cations and two OH^- anionic groups. We have employed Vienna *ab initio* simulation package (VASP) [18] together with the potential projector augmented-wave (PAW) method [19–21]. A Γ-centered optimized 8×8×8 **k**-point mesh was selected for all DFT and GW calculations. To ensure data accuracy and clarity, the calculations were performed within the large plane-wave basis set with 800 eV cutoff, and with the application of GW-versions of PAW Perdew-Burke-Ernzerhof (PBE) pseudopotentials [22], which represent $2p^6 3s^2$, $3s^2 3p^6 4s^2 3d^0$, $2s^2 2p^4$, and $1s^1$ valence electron configurations for Mg, Ca, O and H atoms, respectively. In our computations spin-orbit coupling was not included into consideration. Studies of ground state properties and electronic structure have been performed within the Heyd-Scuseria-Ernzerhof (HSE06) hybrid functional [23–25]. Optical properties have been studied by using the many-body Hedin's GW approximation [26] combined with numerical solution of BSE according to the strategy developed in Refs. [27–29], which utilizes the wave functions derived from hybrid functional calculations as a starting point for subsequent GW numerical procedures. For description of exchange effects in a periodic ion-covalent insulating system we employ the relation $a \approx \epsilon_\infty^{-1}$ (Ref. [30–34]) that approximates the mixing coefficient a (fraction of the Fock exchange) in the xc potential in terms of the effective screening of the bare nonlocal exchange part of the electron-electron interaction [31, 35].

3. Results

In our study, we start with preliminary series of calculations in order to ascertain the relevant value of a via ϵ_∞^{-1} that will consistently be utilized

further as a material-specific parameter related to the short-range Fock exchange in the HSE06 hybrid functional. Detailed considerations concerning numerical and theoretical treatment of the mixing parameter a in terms of ϵ_∞^{-1} can be found in Refs. [34, 36]. Based on that, we could also mention that due to the relation $r_{\rm TF} >> (2/\mu)$, which is common to ion-covalent insulators, such a parametrization is generally safe for tuning the optimal a (here $r_{\rm TF}$ is the Thomas-Fermi screening length and μ characterizes the range separation in the HSE06 hybrid functional). Evaluation of the mixing coefficient a was carried out according to the iterative procedure as follows: First, lattice relaxation has been performed and dielectric properties was studied within the PBE-GGA. Then the macroscopic dielectric tenzor was evaluated using the density functional perturbation theory [37]. Taking these elements as initial guess for a via ϵ_∞^{-1} ($\epsilon_\infty = (2\epsilon_\infty^{xx} + \epsilon_\infty^{zz})/3$), improvements to the macroscopic dielectric matrix was obtained by using a as argument in the modified HSE06 hybrid functional. The calculated ϵ_∞ and a are provided in Table 1. In these calculations the local field (LF) effects have been included into consideration. The subsequent self-consistent electronic structure calculations were carried out using the relaxed lattice geometries within the HSE06 functionals and the mixing parameters a of Table 1.

Table 1: Calculated macroscopic dielectric matrix and fraction of the Fock exchange mixing coefficient a.

Compound		ϵ_∞^{xx}	ϵ_∞^{zz}	ϵ_∞	a
$Mg(OH)_2$	PBE:	2.63	2.60	2.62	
	HSE06:	2.34	2.38	2.35	0.425
$Ca(OH)_2$	PBE:	2.73	2.52	2.66	
	HSE06:	2.36	2.26	2.33	0.429

Fig. 1 displays band structure as well as orbital and site projected density of states (PDOS). The energies of three valence bands (VB) and two conduction bands (CB) as well as the symmetry classification of the bands at the Γ point are listed in Table 2. Analysis shows that $X(OH)2$ are direct band gap materials with the VB maximum and CB minimum located at the Γ-point. Topmost part of the VB shows splitting into two oxygen-derived subbands. One is twofold degenerate p_x, p_y bands and the other one is non-degenerate p_z bands denoted by E_{v1}, E_{v2} and E_{v3}, respectively. Double degeneracy of the p_x, p_y orbitals is lifted along the Γ-K and Γ-M directions, but it conserves

along the Γ-A direction.

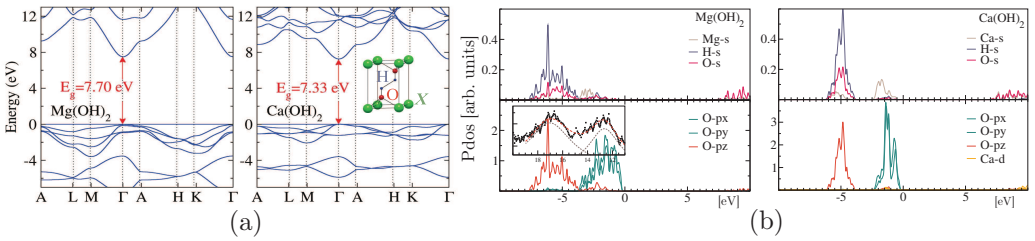

Figure 1: (Color online) Band structure and PDOS for $X(OH)2$. Topmost VB is set to zero. PDOS for $Mg(OH)_2$ has been compared to the experimentally measured XPS spectra [38] plotted in the inset by $(\cdots)$ and interpolated (solid lines).

Table 2: Energies (in eV) of the VB and CB edges near to the fundamental band gap and their symmetry classification at the Γ point (in curly brackets).

Band	$Mg(OH)_2$: Γ	$Ca(OH)_2$: Γ
E_{v3}	$-3.41(A_{2u}+A_{1g})$	$-3.61(A_{2u}+A_{1g})$
E_{v2}	$-0.79(E_u)$	$-1.21(E_u)$
E_{v1}	$0(E_u)$	$0(E_u)$
E_{c1}	$7.70(A_{1g}+A_{2u})$	$7.33(A_{1g}+A_{2u})$
E_{c2}	$11.84(A_{1g}+A_{2u})$	$11.56(A_{1g})$

It follows from Fig. 1 that contribution of s-, p-, and d-states into PDOS significantly differ each from other. One can see that the Mg/Ca atoms donate their valence s-electrons to the O atoms which results in dominance of the oxygen $2p$ orbitals and partially the hydrogen s orbitals in the VB, whereas the lowest empty states of the CB belong mainly to Mg/Ca and O s-type orbitals. They are also responsible for the fundamental band gaps of 7.70 and 7.33 eV for $Mg(OH_2)$ and $Ca(OH_2)$, respectively, corresponding to transitions from O $2p_x$ and $2p_y$ states.

Strong sp_z hybridization between H and O orbitals repels drastically the $2p_z$ bands toward lower energies. Electron localization function analysis has shown that such asymmetry in local angular characters of $2p$-states is rooted in overlapping two chemical interactions as follows: the electron transferred to the O atom along Mg−O/(Ca−O) connections is more likely to stay away from the charge-transfer channel to support a classical ionic bond, i.e. an electrostatic interaction of the anionic hydroxyl group with the metal cation

in the xy plane. The other electron, which was contributed by the hydrogen atom, remains located inside the OH^- ion to be employed mostly in covalent O−H bond along z axis. This leads to an embedding of covalent bonding into the elemental framing of the ionic structure, stipulating thus the splitting of an angular character of the oxygen electronic states.

Calculated PDOS for $Mg(OH)_2$ projected on O atoms [Fig. 1] are in a good agreement with the experimentally measured X-ray photoelectron spectra (XPS) [38] in the energy range 0-8 eV. This allows us to ascribe the two adjacent XPS peaks located at 12.7 eV and 17.0 eV to the O $(2p_x, 2p_y)$ and $2p_z$ states, respectively. It is interesting to note that the energy difference between midpoints of the experimentally measured peak widths match well with the results of our calculations.

From the electron band picture one can reveal two main channels of electric-dipole transitions differing significantly in character: the one stems from the oxygen $(2p_x, 2p_y)$ orbitals providing the direct band gap transitions, whereas the second forms the transition channel that is associated with the hybridized $2p_z$ and s orbitals and becomes pronounced at higher exciting energies. Due to the lack of any noticeable d-related contributions near the fundamental absorption edge one can suggest that the polarization dependencies of the dipolar part of the target optical spectra in this region will mainly differ according to dipolar selection rules connected with the $(2p_x, 2p_y)$ and p_z oxygen states, respectively. Correspondingly, in the region of the higher energies where Ca $3d$-related states become sufficiently large, the dipole transition matrix element will begin additionally to select these states correcting thus the polarization dependencies from p-type orbitals.

We have studied optical properties of $X(OH)2$ for the photon energy range 0-15 eV within the frequency-dependent GW_0 method as implemented in VASP [27, 39–41]. Our G_3W_0 calculations have been performed by using HSE06 electronic-structure descriptions as a starting point. Figure 2 displays the imaginary part of the macroscopic dielectric constant. Analysis shows that $\Im\epsilon_{xx}(\omega)$ and $\Im\epsilon_{zz}(\omega)$ differ from each other significantly. It indicates anisotropy in the optical properties of $X(OH)2$. Strong bound and resonance exciton-related peaks are seen in the $\Im\epsilon_{xx}(\omega)$ spectra inside the band gap and in the CB, respectively. One of the experimentally measurable parameters allowing to confirm existence excitons is reflectivity spectra $R(\omega)$ plotted in the inset of Fig. 2 where one can see strong excitonic peaks.

In order to explain the anisotropy of the optical properties, it could be helpful to look at Fig. 1 in terms of the orbital splitting of the oxygen va-

lence states, presuming that just the longitudinal components of $\epsilon_2(\omega)$ refer to the fundamental absorption edge. Next we recall a fact well-known for polar semiconductors and, especially, for insulators that the dielectric function calculated in the independent-particle approximation is not so accurate as that obtained with accounting for the LF effects. From Fig. 2 we can see the distinct difference between these two types of calculations – the account for the LF effects changes both the peak positions and their intensities in the absorption spectra of the hydroxides significantly. A further point to be made is that the peak positions and mostly the intensities of the electron transitions observed in the $G_3W_0 - BSE$ optical spectra of Fig. 2 are, due to effects of the strong electron-hole coupling, substantially changed in comparison with the noninteracting ones. This implies formation of a bound exciton which corresponds to a new high spectral peak lying lower in energy than the fundamental band gap. Theoretical predictions of these gaps along with the main characteristics of the exciton branch of the optical spectra are summarized in Table 3. Analysis shows that the G_3W_0 quasiparticle band gaps look comparable (slightly larger) with those obtained within the HSE06 functional. This agreement gives us a reasonable confirmation that for $X(OH)2$ the HSE06 wave functions and eigenvalues represent a good starting point for GW numerical procedures.

Table 3: Calculated fundamental band gaps, E_g, and exciton peaks (in eV) in the optical spectra. MBJ stands for the band gap prediction performed with the modified Becke-Johnson potential [42, 43].

Compound	PBE	HSE06m	MBJ	G_3W_0	E_1^{exc}	E_2^{exc}
$Mg(OH)_2$	3.83	7.70	7.16	8.26	7.24	7.83
$Ca(OH)_2$	3.76	7.33	7.20	7.55	6.48	7.09

Our last step is proper interpretation of excitonic signatures seen in the optical spectra of Fig. 2. Analysis of PDOS [Fig. 1] shows that mainly the combination of oxygen and metal are responsible for the excitons possessing largest binding energy. In terms of characters of the electronic states centered either on oxygen anion or metal cation the following two assignments of one-photon vertical transitions to low-lying excited states can be made: (i) the intra-"molecular" transition $O^{2-} \rightarrow O^{2-}$ with the excited configuration $2p_z^2 2p_{x,y}^3 3s^1$, since OH^- sp_z bonding orbitals are situated significantly below, low-lying excited states correspond to planar electronic excitations relating

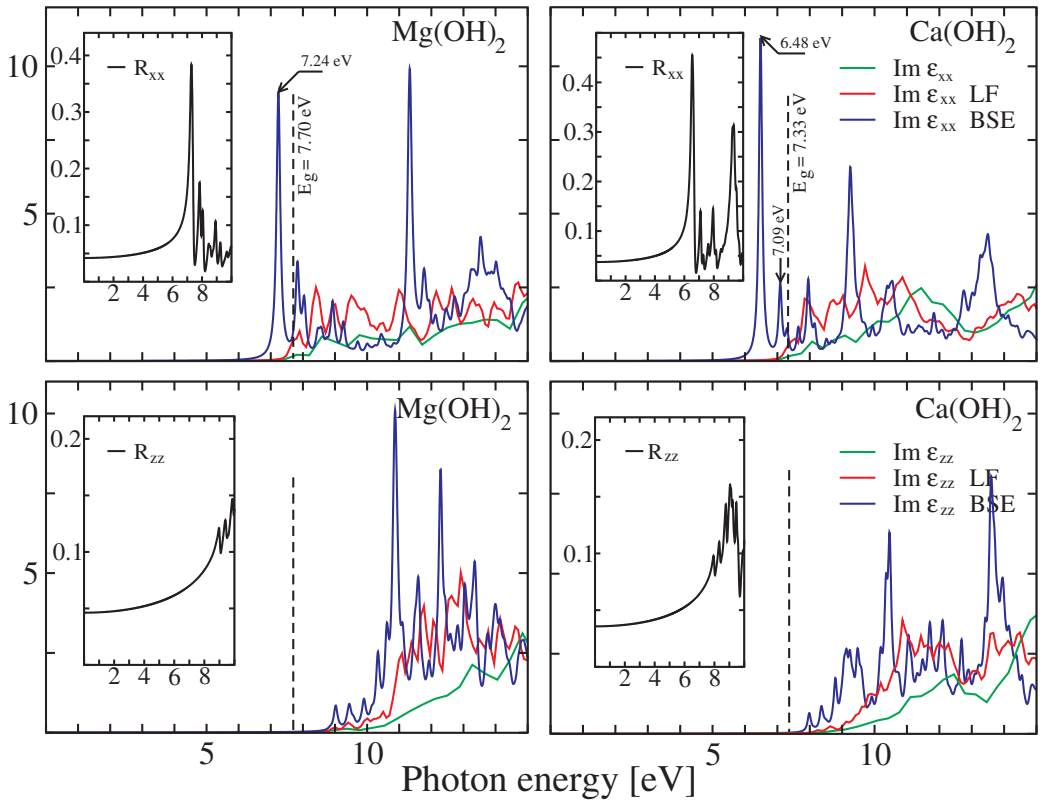

Figure 2: (Color online) The imaginary part of the macroscopic dielectric constants calculated in the independent-particle approximation (i) without and (ii) with inclusion of LF effects, and (iii) within the $G_3W_0 - BSE$ approach. The latter method has been used for calculation of the reflectivity spectra $R(\omega)$ plotted in the inset.

to oxygen of the hydroxyl anion, and (ii) the transition $O^{2-} + X^{2+} \rightarrow O^{-} + X+$ with the excited configurations $2p^5$ and $3p^6 4s^1$ for O and X, respectively; this nonlocal (off-site) transition deals with the induced backward charge transfer along Mg−O connection and is associated with the partial decrease of the $p_{x,y}$ electron density on the oxygen and the proportionate increase of the s electron density on the metal cation. Thus, the central spectral feature is splitting of the excitonic branch of Fig. 2 between two prominent peaks of different intensity, which can be regarded as follows: the larger peak at 7.24 eV (6.48 eV for $Ca(OH)_2$) corresponds to the strong molecular component of the electron-hole state localized at the oxygen of the hydroxyl anion, whereas the origin of the smaller one at 7.83 eV (7.09 eV) is suggested to be much

closer to the electron-hole pair separated on the nearest-neighbors Mg−O.

In order to explain the strong excitonic binding in the hydroxides we refer mainly to a rigorous physical picture established for ion-covalent compounds – the more the electronic charge is localized, the greater strength many-body contributions exert [11, 44]. In this context, aside from the standard feature of the weak screening in the hydroxides we would emphasize the key role of the unoccupied O^{2-} s-type orbitals located in the bottommost CB and hybridized with metal cation s orbitals, which, according to Ref. [11], significantly strengthen the Coulomb and exchange parts of the electron-hole interaction.

4. Summary

In summary, we have presented the first-principles description of the electronic structure and optical properties of multifunctional hydroxides $X(OH)2$ by using DFT calculations with HSE06 hybrid functional and many-body calculations with GW-BSE. Within the frameworks of the combined theoretical approach we have found an intimate connection between the crystal-chemical properties and the relevant features of the electronic spectra. With respect to the optoelectronic properties of $Mg(OH)_2$ and $Ca(OH)_2$ this has allowed us to provide rationalization for a strong Coulomb attraction between an excited electron and a hole and thereby to predict for the first time the existence of excitonic states possessing large binding energy. Imaginary part of the dielectric function and reflectivity spectra show strong peaks corresponding to the bound excitons. The hexagonal lattice environment has an ultimate effect on the excitonic states making their structure highly anisotropic and directly dependent on the polarization of the incident light in such a way that it can be realized only in the $a-b$ plane. We have identified and analyzed the origin of the excitons, which can be attributed to strong localization of the hole and electron to oxygen $2p_x, 2p_y$ occupied states as well as to oxygen and earth metal s empty states, respectively. Our results are expected to initiate further experimental and theoretical studies of $Mg(OH)_2$ and $Ca(OH)_2$. Also our theoretical results can serve as solid input data for developing different experimental designs and synthesis based on the $X(OH)2$ hydroxides.

Acknowledgement

This work has received financial and supercomputing support from the Research Council of Norway through the ISP project 181884. This work was

also supported by the European Union through the European Regional Development Fund (Centre of Excellence "Mesosystems: Theory and Applications", TK114) and by the Estonian Science Foundation grant No 7296. The authors wish to thank Professor Y. Galperin, University of Oslo, Oslo, Norway and Professor M. Ganchenkova, National Research Nuclear University, Moscow, Russia for critical reading of the manuscript and useful comments as well as Dr. Ø. Nordseth, Institute for Energy Technology, Kjeller, Norway for practical help.

References

[1] M. Rohlfing, S. G. Louie, Electron-hole excitations in semiconductors and insulators, Phys. Rev. Lett. 81 (1998) 2312–2315.

[2] M. Rohlfing, S. G. Louie, Electron-hole excitations and optical spectra from first principles, Phys. Rev. B 62 (2000) 4927–4944.

[3] S. M. Menke, R. J. Holmes, Exciton diffusion in organic photovoltaic cells, Energy Environ. Sci. 7 (2014) 499–512.

[4] S. W. Koch, M. Kira, G. Khitrova, H. M. Gibbs, Semiconductor excitons in new light, Nat. Mater. 5 (7) (2006) 523–531.

[5] G. D. Scholes, G. Rumbles, Excitons in nanoscale systems, Nat Mater 5 (9) (2006) 683–696.

[6] R. C. Whited, W. C. Walker, Exciton spectra of cao and mgo, Phys. Rev. Lett. 22 (1969) 1428–1430.

[7] A. Pishtshev, S. Z. Karazhanov, M. Klopov, Chemical bonding in multifunctional hydroxides *xoh*2, Under preparation.

[8] L. X. Benedict, E. L. Shirley, R. B. Bohn, Optical absorption of insulators and the electron-hole interaction: An *Ab Initio* calculation, Phys. Rev. Lett. 80 (1998) 4514–4517.

[9] S. Albrecht, L. Reining, R. Del Sole, G. Onida, *Ab Initio* calculation of excitonic effects in the optical spectra of semiconductors, Phys. Rev. Lett. 80 (1998) 4510–4513.

[10] D. Y. Qiu, F. H. da Jornada, S. G. Louie, Optical spectrum of mos_2: Many-body effects and diversity of exciton states, Phys. Rev. Lett. 111 (2013) 216805.

[11] M. Dvorak, S.-H. Wei, Z. Wu, Origin of the variation of exciton binding energy in semiconductors, Phys. Rev. Lett. 110 (2013) 016402.

[12] H. Miyazaki, R. Mikami, A. Yamada, M. Konagai, Chemical-bath-deposited zno and mg(oh)(2) buffer layer for cu(inga)se-2 solar cells, Jpn. J. Appl. Phys., Part 1 45 (4A) (2006) 2618–2620.

[13] J.-H. Yum, S. Nakade, D.-Y. Kim, S. Yanagida, Improved performance in dye-sensitized solar cells employing tio2 photoelectrodes coated with metal hydroxides, J. Phys. Chem. B 110 (7) (2006) 3215–3219.

[14] C.-H. Huang, Y.-L. Jan, W.-C. Lee, Investigation of mg(o,oh) films prepared by chemical bath deposition as buffer layers for cu(in,ga)se2 solar cells, J. Electrochem. Soc. 158 (9) (2011) H879–H888.

[15] L. Desgranges, G. Calvarin, G. Chevrier, Interlayer interactions in $Mg(OH)_2$: a neutron diffraction study of $Mg(OH)_2$, Acta Crystallogr., Sect. B: Struct. Sci. 52 (1) (1996) 82–86.

[16] W. R. Busing, H. A. Levy, Neutron diffraction study of calcium hydroxide, J. Chem. Phys. 26 (3) (1957) 563–568.

[17] L. Desgranges, D. Grebille, G. Calvarin, G. Chevrier, N. Floquet, J. C. Niepce, Hydrogen thermal motion in calcium hydroxide: $Ca(OH)_2$, Acta Crystallogr., Sect. B: Struct. Sci. 49 (5) (1993) 812–817.

[18] G. Kresse, J. Furthmüller, Efficient iterative schemes for ab initio total-energy calculations using a plane-wave basis set, Phys. Rev. B 54 (16) (1996) 11169–11186.

[19] P. E. Blöchl, Projector augmented-wave method, Phys. Rev. B 50 (24) (1994) 17953–17979.

[20] G. Kresse, D. Joubert, From ultrasoft pseudopotentials to the projector augmented-wave method, Phys. Rev. B 59 (3) (1999) 1758–1775.

[21] G. Kresse, J. Hafner, Ab initio molecular dynamics for liquid metals, Phys. Rev. B 47 (1) (1993) 558–561.

[22] J. P. Perdew, K. Burke, M. Ernzerhof, Generalized gradient approximation made simple, Phys. Rev. Lett. 77 (18) (1996) 3865–3868.

[23] J. Heyd, G. E. Scuseria, M. Ernzerhof, Hybrid functionals based on a screened coulomb potential, J. Chem. Phys. 118 (18) (2003) 8207–8215.

[24] A. V. Krukau, O. A. Vydrov, A. F. Izmaylov, G. E. Scuseria, Influence of the exchange screening parameter on the performance of screened hybrid functionals, J. Chem. Phys. 125 (22) (2006) 224106.

[25] T. M. Henderson, J. Paier, G. E. Scuseria, Accurate treatment of solids with the hse screened hybrid, Phys. Status Solidi B 248 (4) (2011) 767–774.

[26] L. Hedin, New method for calculating the one-particle green's function with application to the electron-gas problem, Phys. Rev. 139 (1965) A796–A823.

[27] F. Fuchs, J. Furthmüller, F. Bechstedt, M. Shishkin, G. Kresse, Quasiparticle band structure based on a generalized kohn-sham scheme, Phys. Rev. B 76 (2007) 115109.

[28] T. Körzdörfer, N. Marom, Strategy for finding a reliable starting point for G_0W_0 demonstrated for molecules, Phys. Rev. B 86 (2012) 041110.

[29] C. Friedrich, M. Betzinger, M. Schlipf, S. Blügel, A. Schindlmayr, Hybrid functionals and gw approximation in the flapw method, J. Phys.: Condens. Matter 24 (29) (2012) 293201.

[30] A. Alkauskas, P. Broqvist, F. Devynck, A. Pasquarello, Band offsets at semiconductor-oxide interfaces from hybrid density-functional calculations, Phys. Rev. Lett. 101 (2008) 106802.

[31] J. Vidal, S. Botti, P. Olsson, J. F. Guillemoles, L. Reining, Strong interplay between structure and electronic properties in $\mathrm{CuIn}(\mathbf{S},\mathrm{Se})_2$: A first-principles study, Phys. Rev. Lett. 104 (2010) 056401.

[32] A. Alkauskas, P. Broqvist, A. Pasquarello, Defect levels through hybrid density functionals: Insights and applications, Phys. Status Solidi B 248 (4) (2011) 775–789.

[33] M. A. L. Marques, J. Vidal, M. J. T. Oliveira, L. Reining, S. Botti, Density-based mixing parameter for hybrid functionals, Phys. Rev. B 83 (2011) 035119.

[34] J. He, C. Franchini, Screened hybrid functional applied to $3d^0 \rightarrow 3d^8$ transition-metal perovskites la M o_3 (M=sc-cu): Influence of the exchange mixing parameter on the structural, electronic, and magnetic properties, Phys. Rev. B 86 (2012) 235117.

[35] S. Botti, J. Vidal, Energy Generation: Solar Energy, Computational Approaches to Energy Materials, John Wiley & Sons Ltd, 2013, book section 2, pp. 29–69.

[36] J. E. Moussa, P. A. Schultz, J. R. Chelikowsky, Analysis of the heyd-scuseria-ernzerhof density functional parameter space, J. Chem. Phys. 136 (20) (2012) 204117.

[37] M. Gajdoš, K. Hummer, G. Kresse, J. Furthmüller, F. Bechstedt, Linear optical properties in the projector-augmented wave methodology, Phys. Rev. B 73 (2006) 045112.

[38] D. E. Haycock, M. Kasrai, C. J. Nicholls, D. S. Urch, The electronic structure of magnesium hydroxide (brucite) using x-ray emission, x-ray photoelectron, and auger spectroscopy, J. Chem. Soc., Dalton Trans. (12) (1978) 1791–1796.

[39] M. Shishkin, G. Kresse, Implementation and performance of the frequency-dependent *gw* method within the paw framework, Phys. Rev. B 74 (2006) 035101.

[40] M. Shishkin, G. Kresse, Self-consistent gw calculations for semiconductors and insulators, Phys. Rev. B 75 (2007) 235102.

[41] M. Shishkin, M. Marsman, G. Kresse, Accurate quasiparticle spectra from self-consistent gw calculations with vertex corrections, Phys. Rev. Lett. 99 (2007) 246403.

[42] A. D. Becke, E. R. Johnson, A simple effective potential for exchange, J. Chem. Phys. 124 (22) (2006) 221101.

[43] F. Tran, P. Blaha, Accurate band gaps of semiconductors and insulators with a semilocal exchange-correlation potential, Phys. Rev. Lett. 102 (2009) 226401.

[44] Meskini, N., Hanke, W., Mattausch, H.J., Balkanski, M., Zouaghi, M., The absorption spectrum of a heteropolar crystal : the rôle of many-particle effects, J. Phys. France 45 (10) (1984) 1707–1715.